Interference Localization and Mitigation in Synthetic Aperture Radars Using Variable Space-Frequency Filter

Nermine Hendy[1*], *Member, IEEE,* Akram Al-Hourani[1*], *Senior Member, IEEE,* Thomas Kraus[2], Maximilian Schandri[2], Markus Bachmann[2], and Haytham M. Fayek[3], *Senior Member, IEEE*

***Abstract*—Radio Frequency Interference (RFI) in Synthetic Aperture Radar (SAR) is a daunting challenge that affects the SAR sensing reliability and its image quality. To ensure that SAR remains a powerful tool for Earth observation, this paper presents an effective two-dimensional tuneable attenuation space-frequency (azimuth-range) filtration. This framework is based on key components including time-frequency features of level-0 SAR data, radar antenna pattern, and the estimated parameters of the interference signal. Additionally, a signal power localization method is applied to estimate the relative position of the interference source with 95% accuracy to facilitate applying the tuneable filter. Simulated results are obtained using a public open-source spaceborne SAR emulator, SEMUS, for generating emulated clean and contaminated SAR raw data. Furthermore, the filtration framework is successfully tested on real-life interference events on the TerraSAR-X satellite raw data.**

***Index Terms*—Radio frequency interference mitigation, SAR interference, spaceborne SAR.**

I. Introduction

SYNTHETIC Aperture Radar (SAR) technology has revolutionized remote sensing and imaging applications, offering high-resolution, all-weather capabilities for various fields, such as: environmental monitoring, disaster management, and defence [1], [2]. However, SAR systems are susceptible to interference problems that can degrade image quality and compromise the reliability of the collected data. Consequently, it poses significant challenges for applications such as terrain mapping, disaster monitoring, agriculture, and defence.

Anomalies in SAR imaging can originate from a variety of sources, including; unintentional electromagnetic emissions, intentional jamming, multipath propagation, terrestrial radars, and system-induced artifacts. Radio Frequency Interference (RFI) from terrestrial sources stands as a predominant cause of anomalies within SAR systems, leading to various artifacts in the collected data and the final focused images. Due to the limited bandwidth and constrains on real-time processing of the current RFI mitigating techniques for some crtical applications, RFI mitigation encounters increased challenges. Ongoing research and development endeavors are committed to enhancing SAR systems' robustness against interference, fostering their utility in an ever-expanding array of critical domains [3]. Narrow-band RFI (NB-RFI) is particularly critical due to its concentrated power within a narrow spectral band, thus hiding some of the underlying features and reducing the overall quality of the image [4].

Interference mitigation techniques are generally classified as parametric, non-parametric, and semi-parametric. Parametric techniques involve the utilization of mathematical models for characterizing the signal, RFI, or both and subsequently mitigate RFI. In [5], the authors combined a band-stop filter (BSF) with a removed spectrum iterative adaptive approach (RSIAA) aimed at the estimation of RFI parameters, followed by a process of filtration and reconstruction of the filtered spectrum. Modeling the SAR signal as 2D-sparse and the RFI as either a sparse or low-rank model were proposed for airborne SAR in [6] and compared with modelling SAR as 1D-sparse, the signal estimation was improved but adding more computational complexity to the approach. The use of RFI as an additional source of illumination has been suggested in [7], however the method only works if the source produces a radar-like waveform. The effectiveness of parametric approaches largely depends on how accurately these models can represent the SAR signal and RFI which limits the method's versatility, particularly in its capacity to effectively mitigate diverse artifacts. In contrast, non-parametric techniques do not rely on a predefined model for the SAR signal or RFI. Instead, it adaptively mitigates the RFI signal from the SAR echo either by analyzing the data to identify and remove the data components that is affected by RFI or by applying adaptive filtering that adjust their parameters in real-time to minimize the effect of RFI. A mitigation approach was developed in [8] based on statistical test in the SAR spectral domain to detect RFI followed by filtration for the corrupted parts of the spectrum, the method was verified only on airbone SAR data. Semi-parametric techniques represent a hybrid approach in statistical modeling and signal processing, combining elements of both parametric and non-parametric methodologies. The authors in [9] developed an adaptive notch semi-parametric method for mitigating strong RFI events in SAR systems, effectively preserving true scene details with adaptive threshold and sparse regularization demonstrating its efficacy through

This work is partially funded by SmartSAT CRC, whose activities are funded by the Australian Government's CRC Program, through the PhD scholarship program to N. Hendy.

[1] Electronics and Telecommunication, School of Engineering, RMIT University, Melbourne, VIC, Australia.
[2] German Aerospace Center (DLR), Münchener Str. 20, 82234 Oberpfaffenhofen, Germany.
[3] School of Computing Technologies, STEM College, RMIT University, Melbourne, VIC, Australia.
[*] Correspondence: nerminahendy@ieee.org || akram.hourani@rmit.edu.au

experiments on real SAR data.

This paper proposes a novel non-parametric SAR NB-RFI mitigation approach applied on the contaminated raw SAR data (level-0). The approach employs an initial estimation of RFI parameters from SAR data compromised by interference. Subsequently, localization leverages these estimated spectral characteristics of the interference, enabling the precise determination of the RFI's azimuth position within the scanned swath based on the power profile. Utilizing this located position alongside the estimated parameters, a customized complex 2D azimuth-range tuneable attenuation BSF is then applied to the unfocused SAR data. This process effectively eliminates RFI from the SAR's raw data with minimal data loss. To validate this approach, simulated and real SAR data are used for testing. For simulation, SEMUS [10], an end-to-end spaceborne SAR emulator, is utilized to emulate a spaceborne SAR scenario and generate level-0 SAR data. Furthermore, SEMUS is used to inject a controlled RFI signal with predefined parameters, serving as a reliable ground truth for validation purposes. Validation on real data is achieved by applying the proposed approach on a real TerraSAR-X contaminated level-0 SAR data [3].

II. System Model

RFI can be broadly categorized into narrow-band (NB) or wide-band (WB) based on the percentage of the spectral overlap with the SAR signal. As stated previously, RFI originating from terrestrial radars are the most notable form of interference [11]. Generally, NB-RFI signal has different characteristics and parameters compared to the SAR raw data which makes it simpler to detect and mitigate. Such NB-RFI affect raw SAR data at particular frequencies and possibly at particular time instances, with the maximum impact occurring when the satellite's main lobe is pointing towards the terrestrial RFI source. Consequently, the RFI geographic location plays a crucial role in the produced artifacts including its severity and extent.

A. RFI Model

In a SAR system, the signal is transmitted during a designated transmission window with a predefined Pulse Repetition Frequency PRF and pulse width T_p, accordingly the reflected echo is captured during an echo window as shown in Fig. 1. Generally, the SAR rearranges the acquired raw data into a 2D format in both the range direction, known as fast-time t, and cross-range (azimuth) direction, known as slow-time η, to generate the phase history data (PHD), level-0 data. Accordingly, any interference signal will impact the SAR data during these *echo windows* as long as the RFI signal falls within the SAR antenna beamwidth. Therefore, the received contaminated SAR PHD contains useful ground reflections in addition to the interference signal s_I and the noise process n. Assuming a generic time-domain form of a clean received two-dimensional SAR unfocused PHD, $s_\mathrm{r}(t,\eta)$, where the SAR data is arranged according to echo windows to form the 2D SAR data. Considering this arrangement, the

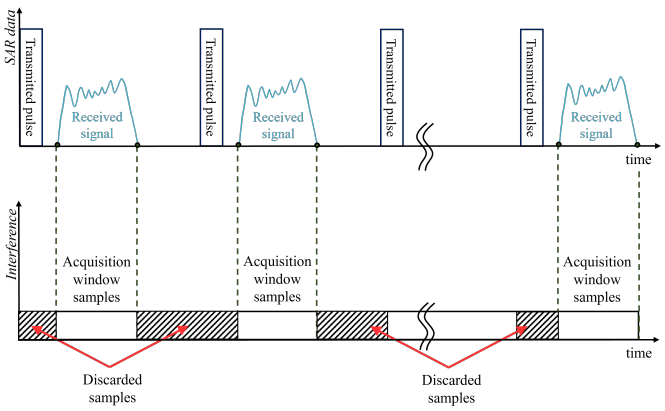

Fig. 1: SAR data and interference signal timing with the effect of the windowing on the interference signal.

interference and noise signals are also rearranged into two-dimensional matrices of the same dimensions as the received signal. Consequently, the contaminated signal $\widetilde{s_\mathrm{r}}(t,\eta)$ can be expressed as follows,

$$\widetilde{s_\mathrm{r}}(t,\eta) = s_\mathrm{r}(t,\eta) + s_\mathrm{I}(t,\eta) + n(t,\eta), \tag{1}$$

where $s_\mathrm{I}(t,\eta)$ and $n(t,\eta)$ are the re-arranged interference and thermal noise signals respectively where the noise is modelled as an additive process with mean $\mu = 0$ and variance σ_n^2, representing the noise power.

B. Channel Model

The signal emitted by an RFI source undergoes attenuation before reaching the SAR platform. This manifest as reduction in the received power due to multiple factors including natural wavefront expansion, atmospheric absorption, and antenna gain pattern. Given the typical operating frequency of the SAR in the C/L/X-bands, the attenuation due to atmospheric absorption can be ignored [12], and the main factor will be the wavefront expansion represented in the free-space path loss. Accordingly, the average received signal power from all rangelines, $\overline{P}_\mathrm{I}$, from an RFI source at the SAR receiving antenna is given by,

$$\begin{aligned} \overline{P}_\mathrm{I} &= \overline{P}_{\mathrm{I}_\mathrm{Tx}} + G_\mathrm{I} + G(\phi_\mathrm{I},\theta_\mathrm{I}) - \overline{\mathrm{FSPL}} && [\mathrm{dB}], \\ \overline{\mathrm{FSPL}} &= \overline{20\log_{10}(R_\mathrm{I})} + 20\log_{10}(f_\mathrm{I}) + 20\log_{10}(\frac{4\pi}{c}) && [\mathrm{dB}], \end{aligned} \tag{2}$$

where $\overline{P}_{\mathrm{I}_\mathrm{Tx}}$ is the average transmitted power of the RFI source, G_I is the antenna gain of the RFI assuming omni-directional and time-invariant antenna, $G(\phi_\mathrm{I},\theta_\mathrm{I})$ is the SAR antenna gain towards the RFI described with the spherical angles ϕ and θ, representing off-boresight angles in the range and cross-range directions respectively, $\overline{\mathrm{FSPL}}$ is the average free space path loss, R_I is the slant distance between the RFI source and the SAR platform, f_I is the RFI center frequency, and c is the speed of light. Since the clean received SAR signal and RFI have vastly different bandwidths, also their power is not constant, we define the Power-Spectral-Density Signal-to-Interference γ as follows,

$$\gamma = 10\log_{10}(\frac{\overline{P}_\mathrm{SAR}/B}{\overline{P}_\mathrm{I}/B_\mathrm{I}}), \tag{3}$$

where $\overline{P}_{\mathrm{SAR}}$ is the average power of the clean received SAR signal and B and B_{I} are the bandwidths of SAR and RFI signals respectively.

III. RFI Localization and Filtration

A. Power-based RFI Localization

For building an effective tuneable filter, we need to estimate the location of the RFI in the azimuth direction. One direct method is to examine the Power Spectral Density (PSD) profile of the contaminated signal across the slow-time. The detailed steps are explained as follows,

Step 1: Estimate the RFI center frequency $\widetilde{f_{\mathrm{I}}}$ (or the center frequency shift estimate $\widetilde{\Delta f} = |f_{\mathrm{o}} - \widetilde{f_{\mathrm{I}}}|$) and the half power bandwidth (HPB) $\widetilde{B_{\mathrm{I}}}$ of the RFI based on the $3\,\mathrm{dB}$ power of the contaminated SAR raw data PSD.

Step 2: Use the estimated parameters to create and apply a complex band-pass filter (BPF) around the estimated center frequency of the RFI. This BPF is applied at each rangeline (azimuth index) to only pass the RFI signal and get more accurate estimation of the RFI location as explained in the next step. The estimated filtered RFI signal will be as follows,

$$\widetilde{s_{\mathrm{I}}}(t,\eta) = s_{\mathrm{r}}(t,\eta) \circledast h(t), \tag{4}$$

where $h(t)$ is the BPF and $\circledast$ is the convolution operator.

Step 3: Following the filtration, the resultant signal predominantly comprises the RFI. The Fast Fourier Transform (FFT) is applied to produce a detailed PSD profile of the RFI, facilitating the estimation of the RFI's location. By analyzing the position of the highest power within this filtered signal, an estimate of the azimuth location of the RFI can be determined.

B. 2D-Spatial-Frequency Filtration

The power received by the SAR antenna changes with the platform movement, accordingly the SIR will change for each azimuth step. Furthermore, the antenna gain pattern shapes the reflected SAR pulses from the swath. Consequently, the RFI signal attenuates the SAR data across the dwell in the same corresponding pattern. Therefore, to be able to filter the RFI optimally with minimal data loss, a tuneable attenuation space-frequency BSF is defined and applied to the contaminated level-0 signal. The defined filter is applied at each rangeline (azimuth index) with certain attenuation according to the SAR azimuth antenna pattern and gain. Hence, the tuneable attenuation coefficients of the proposed BSF are defined based on the received RFI power profile, the calculated SIR, and the SAR antenna gain at the estimated RFI location. From the maximum SAR antenna gain, a maximum attenuation threshold is defined $A_{\max}$ that controls the amount of attenuation at the estimated RFI location to enhance the filtration while the minimum attenuation is $0\,\mathrm{dB}$. From the extracted RFI power profile, a linear relationship between the gain and the required attenuation A_{BSF} is reconstructed as follows,

$$A_{\mathrm{BSF}}(\eta) = (1 - A_{\max})\frac{G(\eta) - G_{\max}}{G_{\max} - G_{\min}} + 1, \tag{5}$$

where $G(\eta)$ is the SAR antenna gain towards RFI at the estimated location, same as in (2), $G_{\max}$ and $G_{\min}$ are the maximum and minimum of this gain respectively. After defining the attenuation coefficients at each azimuth index, the complex space-frequency BSF with the variable attenuation is applied around the estimated frequency shift $\widetilde{\Delta f}$ with the stop-band approximately equal to the estimated RFI bandwidth $\widetilde{B_{\mathrm{I}}}$ in the frequency dimension and equal to the antenna azimuth beamwidth in the azimuth direction.

IV. Simulation and Results

A. Validation Using Simulated Data

An L-band satellite is utilized to generate the SAR unfocused data using SEMUS for fast processing. For generalisation and simplicity and to emulate a controlled RFI signal, a basic Linear Frequency Modulated (LFM) chirp signal from a terrestrial radar is utilized. The parameters to generate the SAR unfocused data, and raw RFI are listed and explained in Table I. Furthermore, the location of the interferer transmitter is defined with respect to the ground reference point GRP (swath center).

The RFI generation process consists of two stages: firstly, defining the RFI signal with the necessary preprocessing steps and secondly, computing the received power at the SAR antenna from the RFI terrestrial transmitter. Firstly, a single demodulated chirp with the predefined parameters is generated. Then the frequency shift Δf between the SAR carrier frequency and the interference carrier frequency is applied to the chirp as shown in Fig. 3a, where the generated shifted chirp from a single pulse $x_{\mathrm{I}}(t)$ is defined as follows,

$$x_{\mathrm{I}}(t) = \prod\left(\frac{t}{T_{\mathrm{pI}}}\right) e^{j\pi(\beta_{\mathrm{I}} t^2 + 2\Delta f t)}, \tag{6}$$

where $\prod$ is the rect function. Subsequently, the generated chirp is repeated for the whole flight duration to create a vector stream of RFI. Afterwards, a temporal hop and stop window is defined and applied to the RFI signal stream. This temporal window segregates the RFI signal in accordance with the sequential acquisition windows throughout the duration of the flight, facilitating the rearrangement of the RFI into a 2D matrix $i(t,\eta)$ of the same size of the SAR data. To accurately emulate the interference signal, it is essential to compute the received power P_{I} from the interferer at the SAR receiving antenna that depends on the predefined γ. To maintain this value, a reference RFI average received power is defined according to $\overline{P}_{\mathrm{I_{Ref}}} = \overline{P}_{\mathrm{SAR}} - \gamma$. According to the previously defined $\overline{\mathrm{FSPL}}$, the required RFI average transmitted power $\overline{P}_{\mathrm{I_{Tx}}}$ to achieve this reference received power will be $\overline{P}_{\mathrm{I_{Tx}}} = \overline{P}_{\mathrm{I_{Ref}}} - L$, where L is the total average loss. Therefore, the final RFI instantaneous received power at the SAR antenna from the calculated transmitted power is calculated according to (2). Finally, the computed received power is applied to the generated interference signal to get the final RFI signal as $s_{\mathrm{I}}(t,\eta) = \sqrt{P_{\mathrm{I}}}\; i(t,\eta)$. Using the proposed approach, the generated RFI signal is injected into level-0 SAR unfocused data before applying the image formation process. Using the Range-Doppler Algorithm (RDA) [10], level-1 contaminated SAR data is obtained as shown in Fig. 2a.

Based on the developed localization approach and using the signal PSD, an estimate of the RFI transmitter frequency shift $\widetilde{\Delta f}$ and bandwidth $\widetilde{B}_{\mathrm{I}}$ are obtained as shown in Fig. 3a. Using the gathered information about the RFI, an estimate of the SAR antenna gain at the RFI is calculated. Due to the projection from the slant range plane to the ground plane, the RFI's azimuth location is re-estimated according to this estimated gain. Therefore, a final estimate of the RFI transmitter azimuth location is computed and compared to the RFI ground truth location as shown in Fig. 4. The estimated azimuth index of the RFI is 1592 while the actual location is 1501 with accuracy of 95% from 500 different scenes with random RFI. The defined 2D-space-frequency tuneable attenuation BSF is shown in Fig. 5, where the attenuation follows the antenna pattern with maximum attenuation at the estimated frequency shift and estimated location. The estimated frequency shift and BW are $7.877\,\mathrm{MHz}$ and $236.5\,\mathrm{kHz}$ respectively. The estimation accuracy of the parameters proves the capability of the proposed approach to achieve proper localization to be used further for filtration. The filtered raw data shown in Fig.3b is highlighting the attenuation of the RFI signal power by approximately $16\,\mathrm{dB}$ where the difference in γ is defined on the figure. Finally, by reapplying the RDA on the obtained filtered signal, a free-of-interference focused level-1 SAR image is obtained as shown in Fig. 2b.

B. Validation Using SAR Data

Finally the proposed approach is tested on real TerraSAR-X raw data from the German Aerospace Center (DLR) to mitigate an actual RFI on SAR image above Los Angeles on October 2015. By applying the proposed approach a clearer focused image is obtained as shown in Fig. 6a and Fig. 6b. Figures 6c and 6d demonstrate the effectiveness of RFI removal, reveals the presence of two vessels that were hidden behind the RFI.

V. Conclusion

This paper introduced an effective tuneable 2D-space-frequency filtration technique to mitigate the interference in synthetic aperture radars. The core concept is to create variable filter attenuation following the power profile of the interfering signal. The filter directly applies on the raw RF signal, which is achieved by accurately estimating azimuthal location of the interferer as the satellite scans the underlying swath. The proposed methodology is tested base on both controlled simulations, and real-world SAR data.

References

[1] A. Tsokas, M. Rysz, P. M. Pardalos, and K. Dipple, "SAR data applications in Earth observation: An overview," *Expert Systems with Applications*, vol. 205, p. 117342, 2022.

[2] R. Del Prete, M. D. Graziano, and A. Renga, "First results on wake detection in SAR images by deep learning," *Remote Sensing*, vol. 13, no. 22, p. 4573, 2021.

[3] M. Schandri, T. Kraus, A. Hourani, N. Hendy, F. Kurnia, and M. Bachmanna, "Analysis of radio frequency interferences in TerraSAR-X products," in *15th European Conference on Synthetic Aperture Radar (EUSAR 2024) (Accepted)*. EUSAR, 2024, pp. 6730–6733.

[4] F. Zhou, M. Xing, X. Bai, G. Sun, and Z. Bao, "Narrow-band interference suppression for SAR based on complex empirical mode decomposition," *IEEE Geoscience and Remote Sensing Letters*, vol. 6, no. 3, pp. 423–427, 2009.

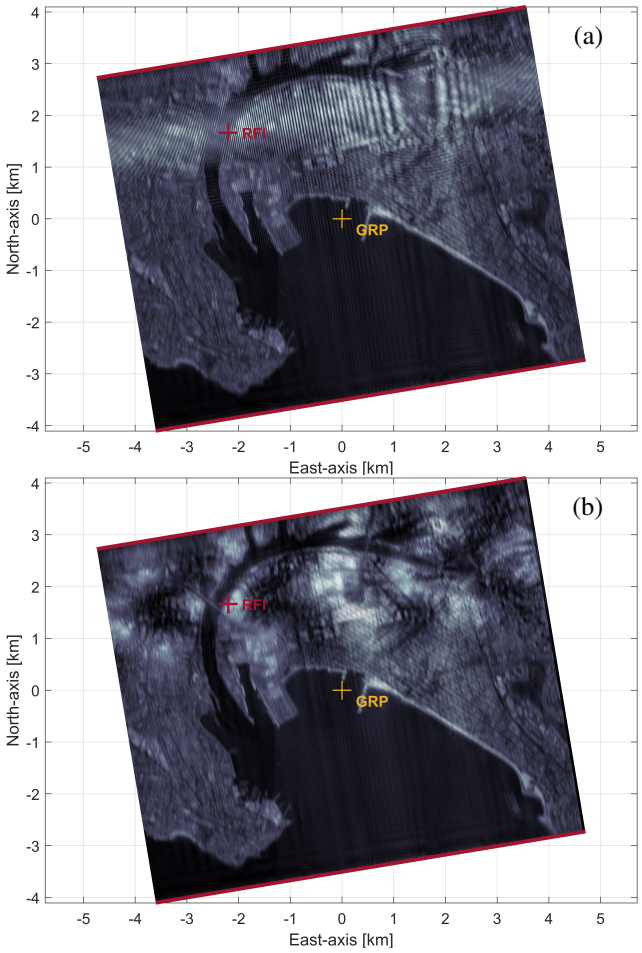

Fig. 2: Focused SAR image, processed with RDA, resulting from a simulated contaminated SAR raw data with simulated RFI, before and after filtration.

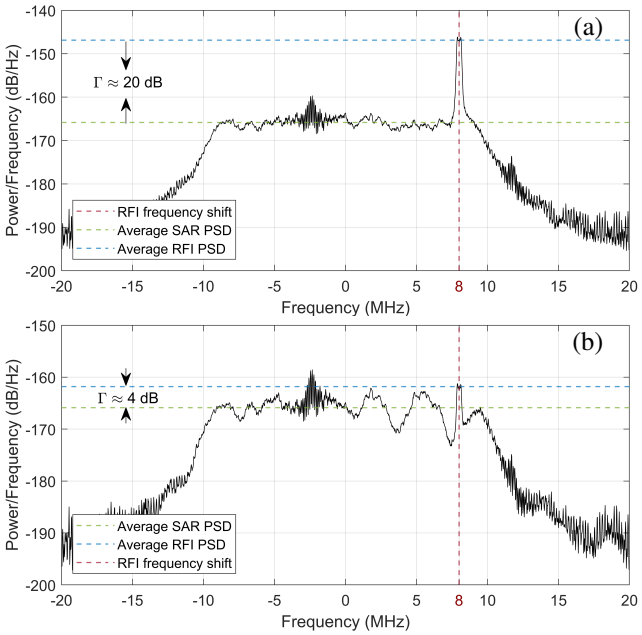

Fig. 3: PSD of SAR raw data before and after RFI removal.

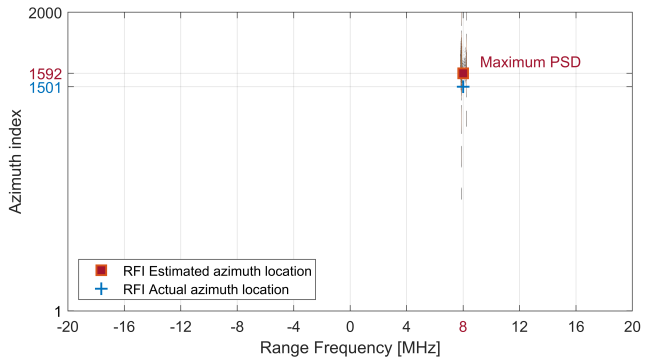

Fig. 4: Estimated location of the RFI source within the swath of the SAR compared with the ground truth location.

TABLE I: SIMULATION PARAMETERS

Parameter	Symbol	Value
SAR Parameters		
Radar Centre Frequency	f_o	1.2 GHz
Wavelength	λ	0.25 m
Pulse repetition frequency	PRF	2 kHz
Pulse repetition Interval	PRI	0.5 ms
Bandwidth	B	20 MHz
Fast-time sampling frequency	f_s	40 MHz
Fast-time sampling time	t_s	25 ns
Pulse width	T_p	5 µs
Doppler frequency	f_d	1 kHz
Transmitted power	P_t	35 dBW
Platform orbital speed	v_s	$7.56\,\mathrm{km\,s^{-1}}$
Interferer Parameters (RFI)		
RFI center frequency	f_I	1.192 GHz
Center frequency shift	Δf	8 MHz
RFI bandwidth	B_I	400 kHz
Duty cycle	D_I	1%
Pulse repetition frequency	$\mathrm{PRF_I}$	200 kHz
Pulse width	T_{PI}	2.5 µs
Chirp rate	β_I	4×10^{12} Hz/s
Transmitter latitude shift	$\Delta\theta_{LAT}$	0.015°
Transmitter longitude shift	$\Delta\theta_{LON}$	−0.025°
Transmitter gain (Isotropic)	G_I	0 dB
Power spectral density-SIR	γ	−20 dB

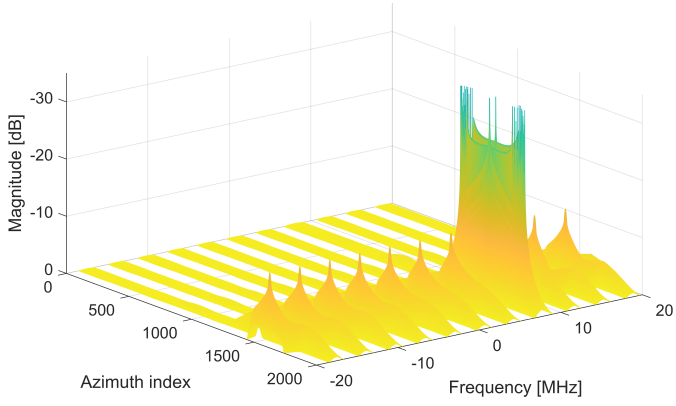

Fig. 5: Magnitude response of the proposed tuneable attenuation 2D complex BPF.

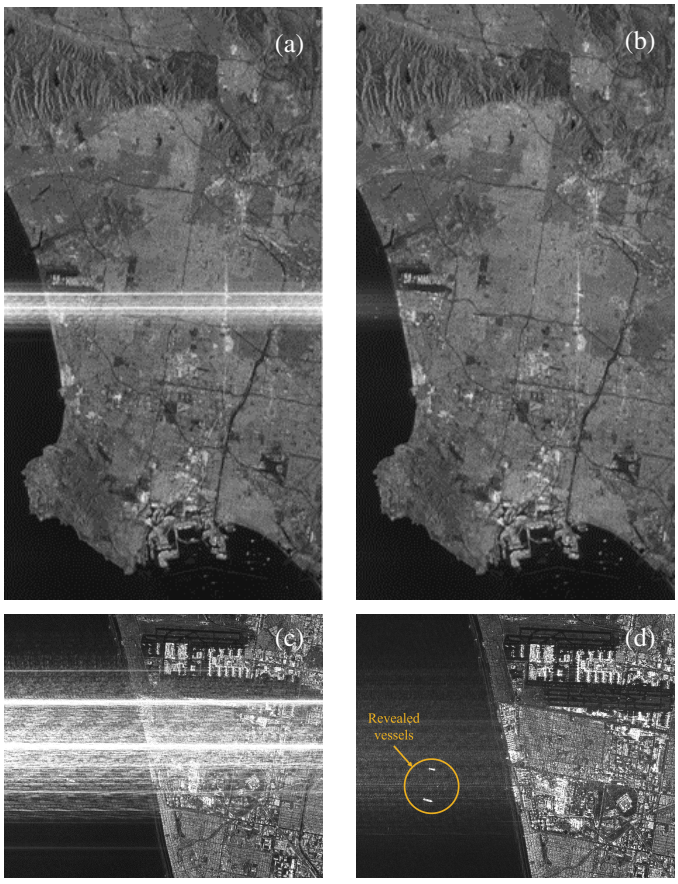

Fig. 6: An actual TerraSAR-X image analyzed by our team. (a) and (b) are respectively the original contaminated images and the filtered image after applying the proposed filtration approach, (c) and (d) are a zoomed-in version revealing ships.

[5] W. Xu, W. Xing, C. Fang, P. Huang, W. Tan, and Z. Gao, "RFI suppression for SAR systems based on removed spectrum iterative adaptive approach," *Remote Sensing*, vol. 12, no. 21, p. 3520, 2020.

[6] S. Joy, L. H. Nguyen, and T. D. Tran, "Joint down-range and cross-range RFI suppression in ultra-wideband SAR," *IEEE Transactions on Geoscience and Remote Sensing*, vol. 59, no. 4, pp. 3136–3149, 2020.

[7] A. Al-Hourani, R. J. Evans, N. Hendy, F. G. Kurnia, M. Bachmann, T. Kraus, and M. Zink, "Hybrid passive-active approach for interference mitigation in spaceborne SAR," in *2023 IEEE International Radar Conference (RADAR)*, 2023, pp. 1–6.

[8] Z. Wang, W. Yu, J. Li, Z. Yu, Y. Zhao, and Y. Luo, "Radio frequency interference mitigation in synthetic aperture radar data based on instantaneous spectrum forward consecutive mean excision," *Remote Sensing*, vol. 16, no. 1, p. 150, 2023.

[9] Y. Mao, Y. Huang, X. Yu, Y. Xin, Y. Wang, and W. Hong, "An radio frequency interference mitigation approach for spaceborne SAR system in low SINR condition," *IEEE Transactions on Geoscience and Remote Sensing*, 2023.

[10] N. Hendy, F. Kurnia, T. Kraus, M. Bachmann, M. Martorella, R. Evans, M. Zink, H. Fayek, and A. Al-Hourani, "SEMUS - an open-source RF-Level SAR emulator for interference modelling in spaceborne applications," *TechRxiv*, 2023. [Online]. Available: https://www.techrxiv.org/doi/full/10.36227/techrxiv.24439942.v1

[11] G. Hajduch, N. Franceschi, M. Pinheiro, and A. Valentino, "SAR-MPC Sentinel-1: Using the RFI annotations," *Sentinel-1 Mission Perform. Center, Saint-Agne, France, Tech. Rep. MPC-0540*, vol. 22, 2022.

[12] A. Al-Hourani and I. Guvenc, "On modeling satellite-to-ground path-loss in urban environments," *IEEE Communications Letters*, vol. 25, no. 3, pp. 696–700, 2020.